

A Lattice Study of the Two-photon Decay Widths for Scalar and Pseudo-scalar Charmonium

Ying Chen,¹ Ming Gong,¹ Ning Li,^{2,*} Chuan Liu,³ Yu-Bin Liu,⁴ Zhaofeng Liu,¹ Jian-Ping Ma,⁵ Yu Meng,⁶ Chao Xiong,⁶ and Ke-Long Zhang⁶
(CLQCD Collaboration)

¹*Institute of High Energy Physics, Chinese Academy of Sciences, Beijing 100049, China*
School of Physics, University of Chinese Academy of Sciences, Beijing 100049, China

²*School of Science, Xi'an Technological University, Xi'an 710032, China*

³*School of Physics and Center for High Energy Physics, Peking University, Beijing 100871, China*
Collaborative Innovation Center of Quantum Matter, Beijing 100871, China

⁴*School of Physics, Nankai University, Tianjin 300071, China*

⁵*Institute of Theoretical Physics, Chinese Academy of Sciences, Beijing 100190, China*

⁶*School of Physics, Peking University, Beijing 100871, China*

In this exploratory study, two photon decay widths of pseudo-scalar (η_c) and scalar (χ_{c0}) charmonium are computed using two ensembles of $N_f = 2$ twisted mass lattice QCD gauge configurations. The simulation is performed two lattice ensembles with lattice spacings $a = 0.067$ fm with size $32^3 \times 64$ and $a = 0.085$ fm with size $24^3 \times 48$, respectively. The results for the decay widths for the two charmonia are obtained which are in the right ballpark however smaller than the experimental ones. Possible reasons for these discrepancies are discussed.

PACS numbers: 12.38.Gc, 11.15.Ha

Keywords: charmonium, decay width, lattice QCD.

I. INTRODUCTION

Charmonium physics plays an important role in the foundation of quantum chromodynamics (QCD) which is believed to be the fundamental theory for the strong interaction. Due to its intermediate energy scale and the special features of QCD, both perturbative and non-perturbative physics show up within charmonium physics [1]. Until now, the best way to study non-perturbative QCD is lattice QCD, a quantum field theory defined on discrete Euclidean space-time. Within this formalism, physical quantities are encoded in various Euclidean correlation functions which in turn can be measured using Monte Carlo simulations [2, 3].

Recently, two photon decay branching fraction for charmonium has been attracting considerable attentions. Theoretically, this quantity is considered to provide a probe for the strong coupling constant at the charmonium scale. It has also been proposed as a sensitive test of the corrections to the non-relativistic approximation via quark models or the effective field theories such as non-relativistic QCD (NRQCD).

In addition, considerable progress has been made in recent years in the physics of charmonia via the investigations from various experimental collaborations, such as, Belle, BaBar, CLEO-c, and BES [4–7]. Generically, there are two ways to measure two-photon branching fraction for charmonium: one is by reconstructing the charmonium in light hadrons with two-photon fusion at e^+e^- machines, the other one is from the $p\bar{p}$ annihilation to

charmonium.

In this paper, we calculate the two-photon decay width of the pseudoscalar and scalar charmonium, i.e. $\Gamma(\eta_c \rightarrow \gamma\gamma)$ and $\Gamma(\chi_{c0} \rightarrow \gamma\gamma)$, in lattice QCD using two ensembles of $N_f = 2$ dynamical twisted mass fermion configurations that were generated by the European Twisted Mass Collaboration (ETMC). This ensures the so-called automatic $\mathcal{O}(a)$ improvement for on-shell observables when the twisted mass fermions are at the maximal twist [8]. Lattice computation for the process $\eta_c \rightarrow \gamma\gamma$ has been done using the same set of configurations in Ref. [9]. In this work, we consider η_c and χ_{c0} simultaneously since they mix with each other due to lattice artifact of $\mathcal{O}(a^2)$.

This paper is organized as follows. In Sect. II, the calculation strategy for the matrix element for two-photon decay of charmonium is reviewed which is then related to the double-photon decay rates. We also outline the strategy for the mass spectrum and form factor of charmonium. In order to improve the signals of the corresponding correlation functions, we apply the variation method to construct the relevant interpolate operators. In Sect. III, the simulation details is divided into several parts: In Sect. III A, we give the parameters relevant with the configurations used in this work. In Sect. III B, mass spectrum of η_c and χ_{c0} are obtained. In Sect. III C, we presents the results of renormalization factor of electromagnetic current operators. In Sect. III D, numerical results of the form factors are presented which are then converted to the two photon decay width of η_c and χ_{c0} . Final results for the decay widths are presented and compared with previous lattice computations and the experiments. The discussion and the conclusion can be found in Sect. IV.

*Corresponding author. Email: lining@xatu.edu.cn

II. STRATEGIES FOR THE COMPUTATION

In this section, we briefly review the methods for the calculation of two-photon decay rate of a charmonium

$$\langle \gamma(q_1, \iota_1) \gamma(q_2, \iota_2) | M(p_f) \rangle = - \lim_{\substack{q'_1 \rightarrow q_1 \\ q'_2 \rightarrow q_2}} \epsilon_\mu^*(q_1, \iota_1) \epsilon_\nu^*(q_2, \iota_2) q_1'^2 q_2'^2 \int d^4x d^4y e^{iq'_1 \cdot y + iq'_2 \cdot x} \langle \Omega | T \{ A^\mu(y) A^\nu(x) \} | M(p_f) \rangle. \quad (1)$$

Here $|\Omega\rangle$ designates the QCD vacuum state; M represents either η_c or χ_{c0} meson state, depending on which one is calculated, and $|M(p_f)\rangle$ is the corresponding meson state with four-momentum p_f , and $|\gamma(q_i, \iota_i)\rangle (i = 1, 2)$ is a single photon state which has the polarization vector $\epsilon(q_i, \iota_i)$

$$\begin{aligned} \langle \gamma(q_1, \iota_1) \gamma(q_2, \iota_2) | M(p_f) \rangle &= (-e^2) \lim_{\substack{q'_1 \rightarrow q_1 \\ q'_2 \rightarrow q_2}} \epsilon_\mu^*(q_1, \iota_1) \epsilon_\nu^*(q_2, \iota_2) q_1'^2 q_2'^2 \int d^4x d^4y d^4w d^4z e^{iq'_1 \cdot y + iq'_2 \cdot x} D^{\mu\rho}(y, z) D^{\nu\sigma}(x, w) \\ &\times \langle \Omega | T \{ j_\rho(z) j_\sigma(w) \} | M(p_f) \rangle \end{aligned} \quad (2)$$

with $D^{\mu\nu}(y, z)$ being the free photon propagator. Basically, each initial/final photon state in the problem is replaced by the corresponding electromagnetic current operator that couples to the photon. Finally, one needs to compute a three-point function of the form $\langle \Omega | T \{ j_\rho(z) j_\sigma(w) \} | M(p_f) \rangle$ which is non-perturbative in

which was presented in Ref. [10]. According to Lehmann-Symanzik-Zimmermann (LSZ) reduction formula, we can express the amplitude for two-photon decay of charmonium in the following form:

with four-momentum q_i and the helicity ι_i . Then, treating QED part perturbatively, we can replace the photon field operators by their corresponding current operators in QCD. We finally arrive at the following equation at the lowest order of QED,

nature and can be computed using lattice QCD methods.

Under certain conditions, Eq. (2) can be analytically continued from Minkowski space to Euclidean space, yielding

$$\begin{aligned} \langle \gamma(q_1, \iota_1) \gamma(q_2, \iota_2) | M(p_f) \rangle &= \lim_{t_f - t \rightarrow \infty} e^2 \frac{\epsilon_\mu(q_1, \iota_1) \epsilon_\nu(q_2, \iota_2)}{Z_M(p_f) 2E_M(p_f)} \int dt_i e^{-\omega_1(t_i - t)} \\ &\langle \Omega | T \left\{ \int d^3\vec{x} e^{-i\vec{p}_f \cdot \vec{x}} \varphi_M(\vec{x}, t_f) \int d^3\vec{y} e^{i\vec{q}_2 \cdot \vec{y}} j^\nu(\vec{y}, t) j^\mu(\vec{0}, t_i) \right\} | \Omega \rangle, \end{aligned} \quad (3)$$

where $\varphi_M(\vec{x}, t_f)$ is the field operator for the meson M , $Z_M(p_f)$ is the spectral weight factor of two-point function, ω_1 is the energy for the photon at time-slice t_i , and $E_M(p_f)$ is the energy for corresponding meson with the momentum p_f . Then, the desired amplitude $\langle \gamma(q_1, \iota_1) \gamma(q_2, \iota_2) | M(p_f) \rangle$ can be obtained once the energies $E_M(p_f)$ and the corresponding overlap matrix element $Z_M(p_f)$ are known. These could be obtained from appropriate two-point functions. In this study, we use the variational method to find the optional interpola-

tion operators to create/annihilate the η_c and χ_{c0} meson state [11].

Generally, an operator \mathcal{O}_i^\dagger having definite J^{PC} can produce all QCD eigenstates with the right quantum numbers

$$\mathcal{O}_i^\dagger |\Omega\rangle = \sum_n |n\rangle \langle n | \mathcal{O}_i^\dagger | \Omega \rangle. \quad (4)$$

In order to create the desired hadrons from vacuum effectively, one could employ a basis of interpolators \mathcal{O}_i

that share the same quantum numbers and construct two-point correlation function matrix as follows

$$C_{ij} = \langle \Omega | \mathcal{O}_i(t) \mathcal{O}_j^\dagger(0) | \Omega \rangle. \quad (5)$$

Here, the operators \mathcal{O}_i are color-singlet constructions built from the basic quark and gluon fields of QCD. Then, we can express the correlation functions in the following form:

$$C_{ij} = \sum_n \frac{1}{2E_n} \langle \Omega | \mathcal{O}_i(0) | n \rangle \langle n | \mathcal{O}_j^\dagger(0) | \Omega \rangle e^{-E_n t}.$$

and the optimized interpolators are:

$$\Omega_n^\dagger = \sum_i v_i^n \mathcal{O}_i^\dagger. \quad (6)$$

Therefore, one should obtain the best estimate for the weights v_i^n according to the solution of the following generalized eigenvalue problem

$$C(t)v^n = \lambda_n(t)C(t_0)v^n. \quad (7)$$

Here, $C(t)$ is the $N \times N$ matrix whose elements are the correlation functions $C_{ij}(t)$ constructed from the basis of N operators, v^n is a generalized eigenvector. The generalized eigenvalues, or principal correlators, $\lambda_n(t)$ behave like $e^{-E_n(t-t_0)}$ at large times, and can be used to determine the spectrum of the states. In practice, we solve Eq. (7) independently on each time-slice t , so that for each state n , we obtain a time series of generalized eigenvectors $v^n(t)$. We use v_i^n chosen on a single time-slice to construct the optimized operators in Eq. (6).

Apart from the two-point functions of η_c and χ_{c0} , we also need the three-point functions $G_{\mu\nu}(t_i, t)$ given by:

$$G_{\mu\nu}(t_i, t) = \langle 0 | T \left\{ \int d^3\vec{x} e^{-i\vec{p}_f \cdot \vec{x}} \varphi_M(\vec{x}, t_f) \right. \\ \left. \times \int d^3\vec{y} e^{i\vec{q}_2 \cdot \vec{y}} j^\nu(\vec{y}, t) j^\mu(\vec{0}, t_i) \right\} | 0 \rangle. \quad (8)$$

We simulate $G_{\mu\nu}(t_i, t)$ on lattices across the temporal direction while the sink of the meson is fixed. Then, we repeat this with a varying t_i to integrate over the three point function with an exponential weight $e^{-\omega_1 t_i}$, and then to extract the matrix element in Eq. (3). In particular, we use the optimized interpolators Ω_n in Eq. (6) to create the η_c , ($n = 1$) or χ_{c0} , ($n = 2$) state for the field interpolating operator φ_M in previous formulas.

For the two photon decay of η_c meson, the matrix element $\langle \gamma(q_1, \iota_1) \gamma(q_2, \iota_2) | M(p_f) \rangle$ in Eq. (3) can be parameterized using form factor $F(Q_1^2, Q_2^2)$ as,

$$\langle \gamma(q_1, \iota_1) \gamma(q_2, \iota_2) | M(p_f) \rangle \\ = 2\left(\frac{2}{3}e\right)^2 m_{\eta_c}^{-1} F(Q_1^2, Q_2^2) \epsilon_{\mu\nu\rho\sigma} \epsilon^\mu(q_1, \iota_1) \epsilon^\nu(q_2, \iota_2) q_1^\rho q_2^\sigma \quad (9)$$

where ϵ_1, ϵ_2 are polarization vectors, Q_1^2, Q_2^2 are virtualities and q_1, q_2 are the four-momenta for the two photons.

The corresponding decay width can be expressed in terms of $F(0, 0)$,

$$\Gamma(\eta_c \rightarrow \gamma\gamma) = \pi \alpha_{em}^2 \frac{16}{81} m_{\eta_c} |F(0, 0)|^2 \quad (10)$$

with $\alpha_{em} \simeq 1/137$ being the fine structure constant. Similarly, for χ_{c0} we have another form factor $G(Q_1^2, Q_2^2)$,

$$\langle \gamma(q_1, \iota_1) \gamma(q_2, \iota_2) | M(p_f) \rangle \\ = 2\left(\frac{2}{3}e\right)^2 m_{\chi_{c0}}^{-1} G(Q_1^2, Q_2^2) (\epsilon_1 \cdot \epsilon_2 q_1 \cdot q_2 - \epsilon_2 \cdot q_1 \epsilon_1 \cdot q_2) \quad (11)$$

with the decay width given by

$$\Gamma(\chi_{c0} \rightarrow \gamma\gamma) = \pi \alpha_{em}^2 \frac{16}{81} m_{\chi_{c0}} |G(0, 0)|^2. \quad (12)$$

III. SIMULATION RESULTS

A. Simulation setup

In this work, we utilize two ensembles with $N_f = 2$ (degenerate u and d quarks) twisted mass configurations. These configurations are generated by the ETMC at the maximal twist to implement the so-called automatic $\mathcal{O}(a)$ improvement [8]. The explicit parameters for these ensembles are presented in Ref. [12] and the two ensembles that we utilized are tabulated in Table I. For the

TABLE I: Configuration parameters.

	β	a [fm]	V/a^4	$a\mu_{sea}$	m_π [MeV]	$m_\pi L$	N_{cfg}
Ens. B_1	3.9	0.085	$24^3 \times 48$	0.004	315	3.3	200
Ens. C_1	4.05	0.067	$32^3 \times 64$	0.003	300	3.3	199

valence sector, we adopt the Osterwalder-Seiler setup which amounts to introducing two extra twisted doublets for each non-degenerate quark flavors, namely, (u, d) and (c, c') with twisted masses $a\mu_l$ and $a\mu_c$, respectively [13–17]. The explicit values of $a\mu_l$ on Ens. B_1 is 0.004, and 0.003 for the Ens. C_1 , respectively. In this simulation, we use the physical mass of η_c to set the value of the $a\mu_c$, and the explicit values are 0.2542 and 0.2018 for Ens. B_1 and Ens. C_1 respectively. In each doublet, the Wilson parameters have opposite signs ($r = -r' = 1$). Performing an axial (or chiral) transformation, quark fields in the physical basis transform into the twisted basis [13]; i.e.,

$$\begin{pmatrix} u \\ d \end{pmatrix} = \exp(i\omega\gamma_5\tau_3/2) \begin{pmatrix} \chi_u \\ \chi_d \end{pmatrix} \\ \begin{pmatrix} c \\ c' \end{pmatrix} = \exp(i\omega\gamma_5\tau_3/2) \begin{pmatrix} \chi_c \\ \chi_{c'} \end{pmatrix}, \quad (13)$$

where ω is the twist angle, and $\omega = \pi/2$ represents maximal twist. Then, the left of the above equations correspond to quark fields in the physical basis, and the right correspond to quark fields in the twisted basis.

Before writing out the explicit form of meson operators, one should exploit the symmetry properties of twisted mass LQCD. We will follow the discussion in reference [18] below. Isospin I and parity \mathcal{P} are broken by $\mathcal{O}(a^2)$ effects in twisted mass LQCD. While, a specific combination (i.e. light flavor exchange combined with parity) is still a symmetry of twisted mass LQCD. We first write down the interpolating-field operators in the twisted basis, and build the interpolating operators with the same Wilson parameters [16]. For the purpose of η_c and χ_{c0} , we use two basis operators $\mathcal{O}_1(x) = \bar{c}(x)\gamma_5 c(x)$, $\mathcal{O}_2 = \bar{c}(x)c(x)$. According to Eq. (13), the two basic operators in twisted basis are given by $\mathcal{O}_1 = \bar{\chi}_c \chi_c$ and $\mathcal{O}_2 = \bar{\chi}_c \gamma_5 \chi_c$ which appear to have opposite parity. However, since twisted mass lattice QCD breaks parity, they in fact mix with each other. Taking into account of this mixing is crucial. One needs to go through the solution of the generalized eigenvalue problem in Eq. (7) to obtain the optimized operator that will create the η_c and χ_{c0} meson from the vacuum. Without performing this generalized eigenvalue separation, it is found that the correct signal of χ_{c0} cannot be observed in the two-point functions. The signal of η_c can of course be observed even without considering this mixing effect since it is the lightest state under consideration.

B. Mass spectra for η_c and χ_{c0}

The eigenvalue λ_n in Eq. (7) corresponding with the corresponding meson state, i.e. $n = 1$ represents η_c meson, and $n = 2$ represents χ_{c0} meson. Since, we use the anti-periodic boundary condition,

$$\lambda_n(t, \mathbf{p}_f) \xrightarrow{t \gg 1} \frac{|Z_M|^2}{E_M(\mathbf{p}_f)} e^{-E_M(\mathbf{p}_f) \cdot \frac{T}{2}} \times \cosh \left[E_M(\mathbf{p}_f) \cdot \left(\frac{T}{2} - t \right) \right]. \quad (14)$$

In practical, we use eigenvalue λ_1 with $\mathbf{p}_f = (0, 0, 0)$ to fit the spectral weight Z_{η_c} , and the explicit value of this factor is 0.4416(8) and 0.2675(3) on Ens. B_1 and Ens. C_1 , respectively. While, we use eigenvalue λ_2 with $\mathbf{p}_f = (0, 0, 0)$ to fit the spectral weight $Z_{\chi_{c0}}$, and the explicit value of this factor is 0.6699(71) and 0.2983(33) on Ens. B_1 and Ens. C_1 , respectively. It is easily seen that the mass can also be extracted from,

$$\cosh(m_n) = \frac{\lambda_n(t-1) + \lambda_n(t+1)}{2\lambda_n(t)}, \quad (15)$$

with m_1 being the mass of η_c meson and m_2 being that of χ_{c0} , respectively. The effective mass plateaus of these mesons for Ens. B_1 and Ens. C_1 are illustrated in Fig. 1. From these mass plateaus, the masses of the mesons are determined and the statistical errors are obtained using jackknife method. The numerical results for the masses are summarized in Tab. II. Note that the mass values

for η_c are utilized to fix the valence charm quark mass parameter $a\mu_c$. Therefore, only the mass of χ_{c0} are predictions from this lattice computation.

TABLE II: Mass values for η_c and χ_{c0} on Ens. B_1 and Ens. C_1 respectively. The last line cites the corresponding result from PDG [19].

	η_c	χ_{c0}
Ens. B_1 : Mass[MeV]	2978(1)	3454(6)
Ens. C_1 : Mass[MeV]	2970(1)	3416(13)
PDG: Mass[MeV]	2983.9(5)	3414.71(30)

In principle, glueball states with the same quantum numbers are also present in the similar energy range [20]. However, in this lattice calculation, we have only utilized the quark bilinear operators for the charmonium states and have not observed the sign of the glueballs.

C. Renormalization factor Z_V of electromagnetic current operators

The current operators in Eq. (8) are electromagnetic current operators. In principle, they contain all flavors of quarks weighted by the corresponding charges. Light quark flavors will only enter the question via disconnected diagrams which are neglected in this study. Only considering the charm quark, we only need to consider the current $\bar{c}\gamma_\rho c(x)$. A subtlety in the lattice computation is that, with $c(x)/\bar{c}(x)$ being the bare charm/anti-charm quark field on the lattice, composite operators such as the current $j_\rho(x) = Z_V \bar{c}(x)\gamma_\rho c(x)$ needs an extra multiplicative renormalization factor Z_V which can be extracted by the ratio of two-point function with respect to the three-point function for η_c [21]:

$$Z_V^\mu = \frac{p^\mu}{E(p)} \frac{(1/2)\Gamma_{\eta_c}^{(2)}}{\Gamma_{\eta_c}^{(3)}}, \quad (16)$$

where μ is the Dirac index and we take it to be zero. $\Gamma_{\eta_c}^{(2)}$ and $\Gamma_{\eta_c}^{(3)}$ are two point correlation function and three point correlation function relevant with η_c . The explicit forms are:

$$\begin{aligned} \Gamma_{\eta_c}^{(2)} &= \sum_{\mathbf{x}} e^{-i\mathbf{p}\cdot\mathbf{x}} \langle \mathcal{O}_{\eta_c}(\mathbf{x}, t) \mathcal{O}_{\eta_c}^\dagger(0, 0) \rangle \\ \Gamma_{\eta_c}^{(3)} &= \sum_{\mathbf{x}, \mathbf{y}} e^{-i\mathbf{p}_f \cdot \mathbf{x}} e^{i\mathbf{q} \cdot \mathbf{y}} \langle \mathcal{O}_{\eta_c}(\mathbf{x}, t_f) \bar{c}\gamma_0 c(\mathbf{y}, t) \mathcal{O}_{\eta_c}^\dagger(0, 0) \rangle \end{aligned} \quad (17)$$

with $\mathcal{O}_{\eta_c}^\dagger$ and \mathcal{O}_{η_c} creating and annihilating a state with the quantum number of η_c meson, respectively. Actually, we use the simple local operator, i.e. $\bar{c}\gamma_5 c$. According to Eq. (16), we can obtain the multiplicative renormalization factor Z_V , and show it in Fig. 2. The values of the

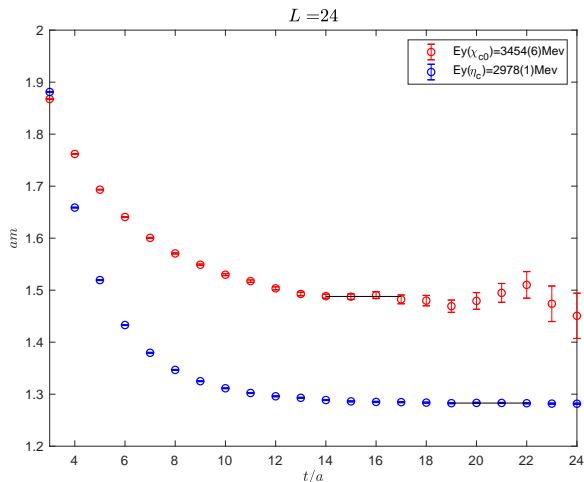
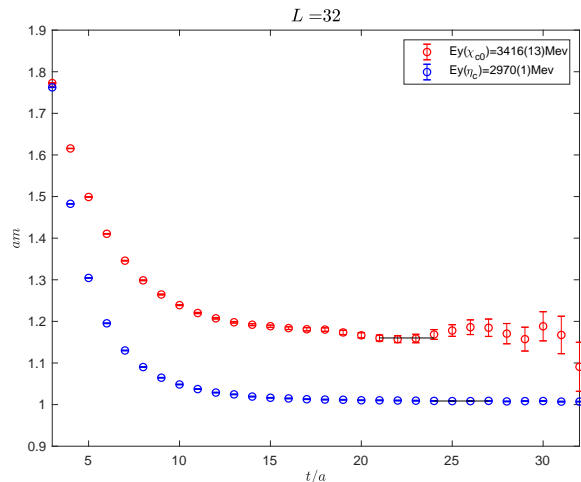
(a) Ens. B_1 (b) Ens. C_1

FIG. 1: Mass plateaus of η_c (blue point) and χ_{c0} (red point) for Ens. B_1 and Ens. C_1 . The horizontal line segments denote the corresponding mass plateaus.

renormalization factor Z_V are 0.6296(18) and 0.6476(61) for Ens. B_1 and Ens. C_1 , respectively.

D. Form factors for two photon decay of η_c and χ_{c0}

To compute the relevant matrix element in Eq. (3), we place the meson at a fixed sink position t_f which is chosen to be 24 for Ens. B_1 and 32 for Ens. C_1 , respectively. These sinks are then used as a sequential source for a backward propagator inversion. This allows us to investigate all possible source positions t_i . We can then freely vary the values of ω_1 , Q_1^2 and inspect the integrand as a function of t_i in Eq. (3) for a given insertion position t . As an example, in Fig. 4 and Fig. 5, we show the integrand for the insertion positions $t = 4, 8, 12, 16, 20$ for Ens. B_1 and $t = 4, 8, 12, 16, 20, 24, 28$ for Ens. C_1 with a particular value $\vec{p}_f = (000)$ for η_c and χ_{c0} .

The computation has to cover the physical interesting kinematic regions. For this purpose, we have to scan the corresponding parameter space of the two virtualities Q_1^2 and Q_2^2 . Basically, we follow the following strategy: we first fix the four-momentum of η_c and χ_{c0} , $p_f = (E, \mathbf{p}_f)$ and place it on a given time-slice $t_f = T/2$. In this simulation, we only compute the case of $\mathbf{p}_f = (0, 0, 0)$, and E is simply the mass of η_c or χ_{c0} meson. Then, we judiciously choose several values of virtuality Q_1^2 around the physical point $Q_1^2 = 0$. To be specific, we picked the range $Q_1^2 \in [-0.5, +0.1] \text{ GeV}^2$ on Ens. B_1 and $Q_1^2 \in [-0.5, +0.1] \text{ GeV}^2$ on Ens. C_1 , which satisfies the constraint $Q_1^2 > -m_\rho^2$ [9]. For a given \mathbf{p}_f , a choice of \mathbf{q}_1 completely specifies \mathbf{q}_2 due to $\mathbf{p}_f = \mathbf{q}_1 + \mathbf{q}_2$. Therefore, we take several choices of $\mathbf{q}_1 = \mathbf{n}_1(2\pi/L)$ by changing three-dimensional integer \mathbf{n}_1 . Then the energy of the first photon is also obtained using either the con-

tinuum or the lattice dispersion relations:

$$\omega_1^2 = \mathbf{q}_1^2 - Q_1^2, \quad (19)$$

$$4 \sinh^2(\omega_1/2) = 4 \sum_i \sin^2(\mathbf{q}_{1i}/2) - \hat{Q}_1^2, \quad (20)$$

where $\hat{Q}_1^2 = 4 \sinh^2(Q_1/2)$ is the lattice version for the virtuality. It turns out that we can also compute the virtuality of the second photon, since both ω_2 and \mathbf{q}_2 are constrained by the energy-momentum conservation. One has to make sure that, the values of Q_2^2 thus computed do satisfy the constraint $Q_2^2 > -m_\rho^2$ otherwise it is omitted. This procedure is summarized as follows:

1. Judiciously choose several values of Q_1^2 in a suitable range. We picked 7 values of Q_1^2 ;
2. Pick different values of \mathbf{n}_1 such that $\mathbf{q}_1 = \mathbf{n}_1(2\pi/L)$. As described above, this fixes both ω_1 and Q_2^2 using energy-momentum conservation. This is done using either the continuum or the lattice dispersion relations. To be specific, for each Q_1^2 , we picked 4 different \mathbf{q}_1 ;
3. Make sure all values of $Q_1^2, Q_2^2 > -m_\rho^2$, otherwise the choice is simply ignored;
4. For each validated choice above, compute the three-point functions (8) and obtain the hadronic matrix element using Eq. (3).

In such a way, we have obtained altogether 28 points on the (Q_1^2, Q_2^2) plane around the origin. As an example, the distribution of these virtualities for the two mesons are shown in Fig. 3 for the case of lattice dispersion relations. One could also do the same thing using the conventional continuum dispersion relations. The difference of these

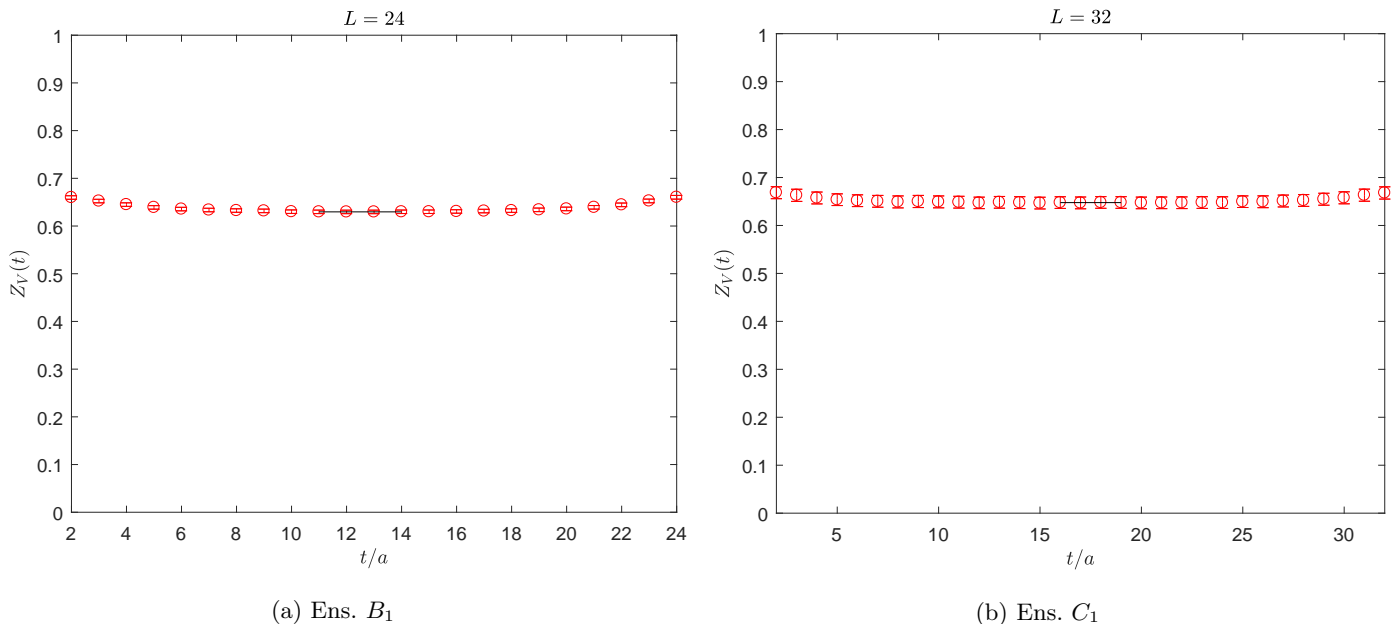


FIG. 2: Renormalization factors Z_V for Ens. B_1 and Ens. C_1 . The horizontal line segments denote the corresponding values for Z_V .

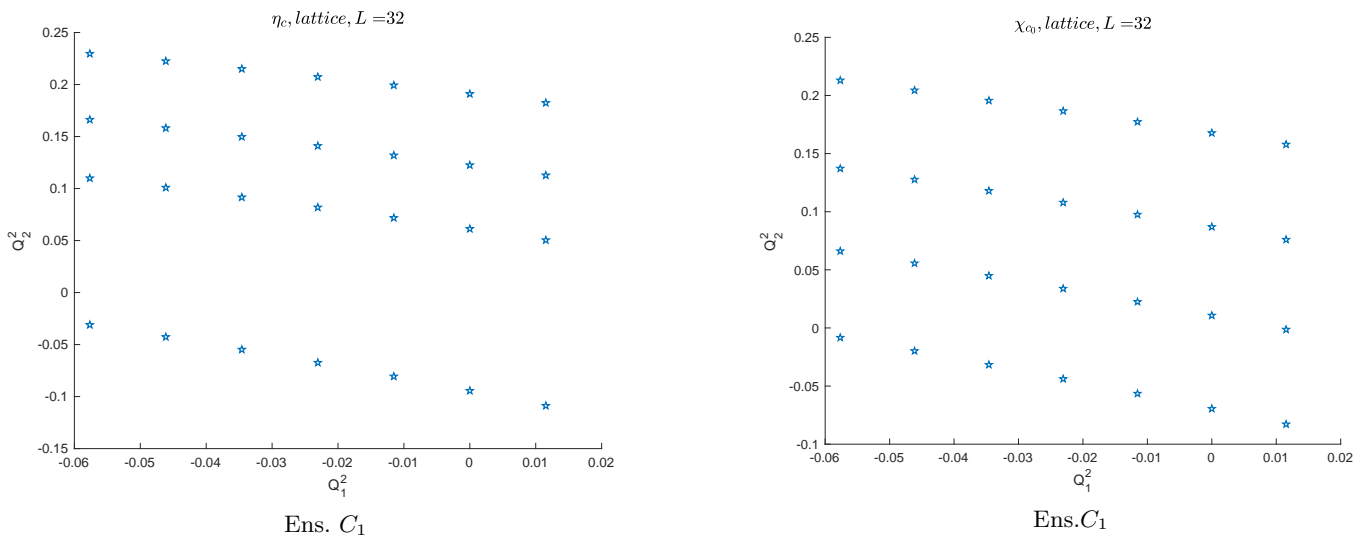


FIG. 3: The distribution of virtualities (Q_1^2, Q_2^2) (lattice units) for Ens. C_1 computed for η_c (left panel) and χ_{c0} (right panel).

two treatments finally will provide us with an estimate for the finite lattice spacing error of the calculation.

In our real lattice QCD computation, the integration of t_i in Eq. (3) are replaced by discrete summation over t_i using trapezoid rule. The resulting values exhibit a plateau behavior with respect to t which is then utilized to extract the corresponding form factor. In such a way, we have obtained numerical results for $F(Q_1^2, Q_2^2)$ and $G(Q_1^2, Q_2^2)$ at 28 different points in the plane of the two virtualities. As an example, the form factor plateaus for η_c are illustrated in Fig. 6 for the case of $Q_1^2 = 0 \text{ GeV}^2$. The corresponding case for χ_{c0} are shown in Fig. 7.

E. Fitting of the form factor and the physical decay widths

To obtain the physical decay width, we only need the values of the form factors at the physical photon point, namely $Q_1^2 = Q_2^2 = 0$. As we have seen in Fig. 3 the distribution of 28 data points in the (Q_1^2, Q_2^2) plane, we could implement cuts in the plane. For a given value of $Q_{\text{cut}}^2 > 0$, we select the points that satisfy the following inequality:

$$\sqrt{(Q_1^2)^2 + (Q_2^2)^2} \leq Q_{\text{cut}}^2. \quad (21)$$

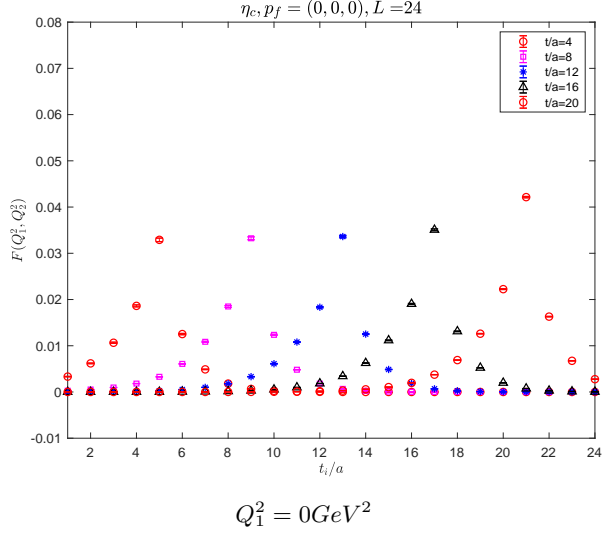
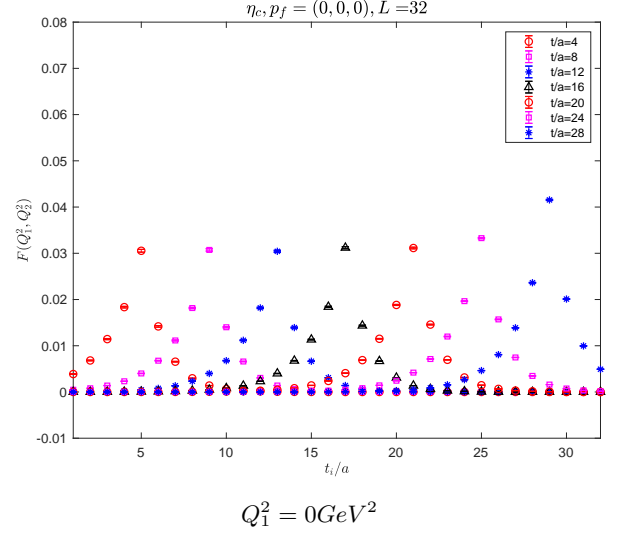
(a) Ens. B_1 (b) Ens. C_1

FIG. 4: The integrand for insertion positions obtained from simulations on Ens. B_1 (left figure), and Ens. C_1 (right figure) respectively. We take $n_2 = (-1 -1 -2)$; $n_f = (0 0 0)$ as an example. The insertion positions for lattice size: $24^3 \times 48$ and lattice size: $32^3 \times 64$ are $t = 4, 8, 12, 16, 20$ and $t = 4, 8, 12, 16, 20, 24, 28$ respectively.

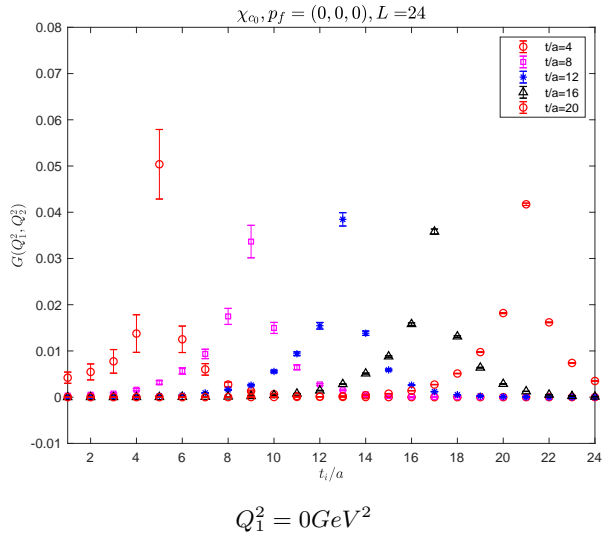
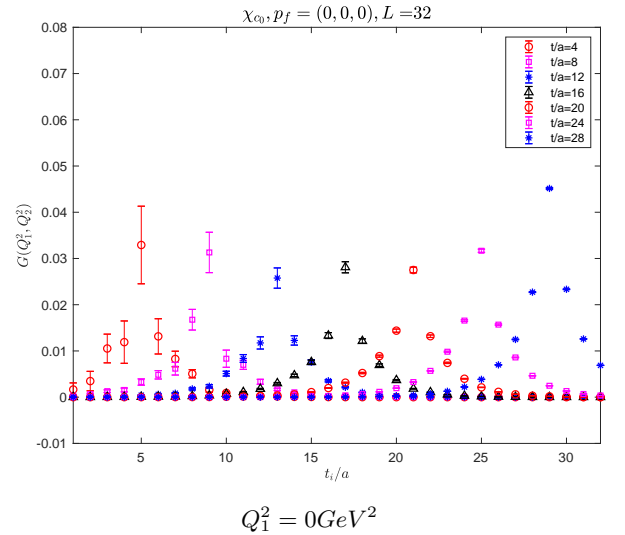
(a) Ens. B_1 (b) Ens. C_1

FIG. 5: The integrand for insertion positions obtained from simulations on Ens. B_1 (left figure), and Ens. C_1 (right figure) respectively. We take $n_2 = (00 -3)$; $n_f = (0 0 0)$ as an example. The insertion positions for lattice size: $24^3 \times 48$ and lattice size: $32^3 \times 64$ are $t = 4, 8, 12, 16, 20$ and $t = 4, 8, 12, 16, 20, 24, 28$ respectively.

Obviously, taking a large enough Q_{cut}^2 will allow all of the points to be considered while selecting a smaller value for Q_{cut}^2 will take into account only those points whose distances are closer than Q_{cut}^2 . On the other hand, for a given value of Q_{cut}^2 , we could utilize different fitting formula to obtain the corresponding values of the form

factor. Since it is the value at the origin that is directly related to the decay width, it is natural to use a polynomial type of fit in both Q_1^2 and Q_2^2 . What is more, due to boson symmetry, this function needs to be symmetric with respect to Q_1^2 and Q_2^2 . Therefore, by varying the cut value Q_{cut}^2 and various orders of polynomials in the

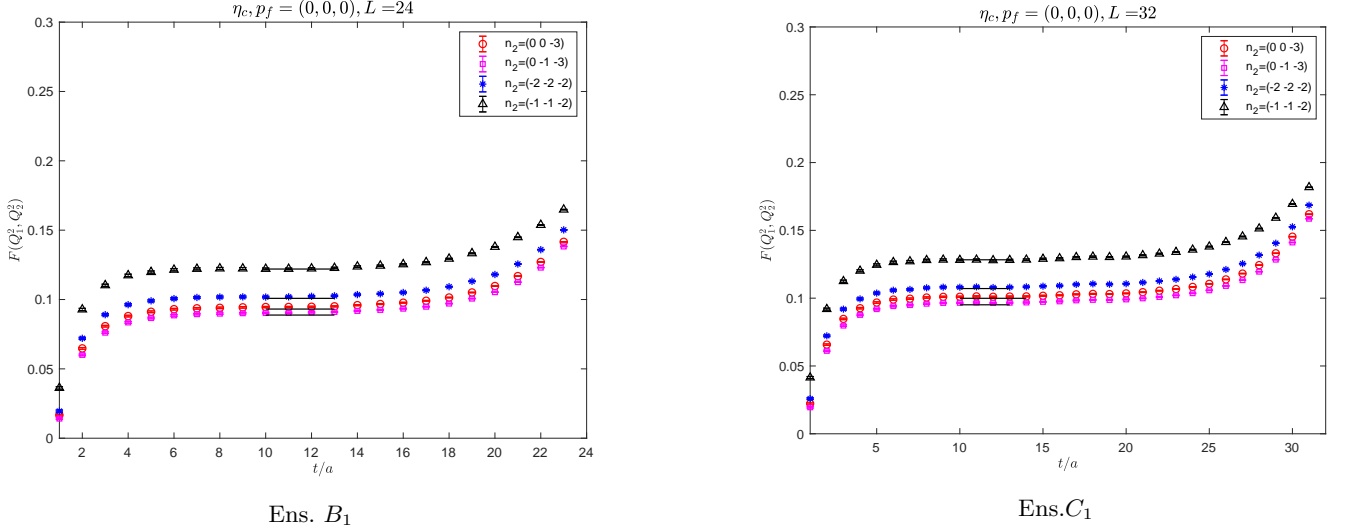


FIG. 6: The plateaus of the pseudoscalar form factors obtained from integration of t_i for three point function $G_{\mu\nu}(t_i, t)$ with Ens. B_1 (left figure), and Ens. C_1 (right figure) respectively. We take $Q_1^2 = 0 \text{ GeV}^2$; $n_f = (0 \ 0 \ 0)$ as an example. The errors in these figures are estimated using the conventional jack-knife method.

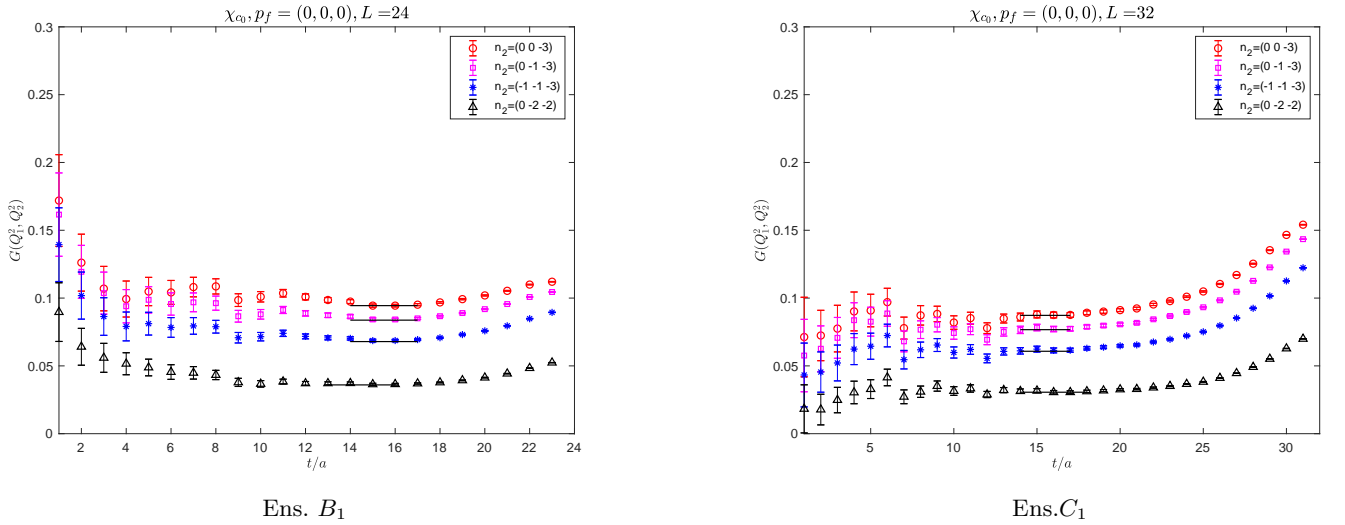


FIG. 7: The plateaus of scalar form factor obtained from integration of varies t_i for three point function $G_{\mu\nu}(t_i, t)$ with Ens. B_1 (left figure) and Ens. C_1 (right figure) respectively. We take $Q_1^2 = 0 \text{ GeV}^2$; $n_f = (0 \ 0 \ 0)$ as an example. The errors in these figures are estimated using the conventional jack-knife method.

virtualities, we could investigate the values of the form factors at the physical point.

To be specific, we adopt a polynomial ansatz up to Q_1^2 and Q_2^2 to the third power to fit the data of the form factor. For η_c meson, we use:

$$\begin{aligned}
 F(Q_1^2, Q_2^2) &= a_0 + a_1(Q_1^2 + Q_2^2) \\
 &+ a_2(Q_1^4 + Q_2^4) + a_3Q_1^2Q_2^2 \\
 &+ a_4(Q_1^6 + Q_2^6) + a_5(Q_1^2Q_2^4 + Q_2^2Q_1^4) \quad (22)
 \end{aligned}$$

and a similar form for the χ_{c0} form factor $G(Q_1^2, Q_2^2)$. Note that $a_0 \equiv F(0, 0)$ is the form factor at the physical photon point which is directly related to the decay

width of the meson. Polynomial forms with less terms, i.e. with only up to first or second powers in Q_1^2 and Q_2^2 , have also been attempted. Note that this implies that we are fitting the data points with 2, 4 and 6 parameters, respectively since terms at the same orders of Q_1^2 and Q_2^2 should be included or excluded on the same footing. In all cases, correlated fits are performed. Depending on the number of points taken into account which is controlled by Q_{cut}^2 , and the number of terms kept in the fitting polynomial, we finally arrive at the values for the form factors at the origin, namely $F(0, 0) = a_0$ for both ensembles. Similar procedures have been implemented as well for χ_{c0} , resulting in the values for $G(0, 0)$.

The fitting procedures described above can be implemented using either the continuum or lattice version of the dispersion relations as indicated in Eq. (19) or Eq. (20). The procedure can be carried out for either pseudo-scalar or scalar meson on either of the two ensembles utilized in this calculation. Therefore, we carry out the fitting procedure in 8 different cases. The difference between the corresponding results obtained from different dispersion relations will then inform us about lattice artifacts of the calculation.

As an illustration, in Fig. 8, the fitting results for η_c and χ_{c0} on Ens.C1 using lattice dispersion relations are shown. Here the horizontal axis denotes the cut values Q_{cut}^2 while the vertical axis indicates the values for $F(0,0)$ or $G(0,0)$ together with the errors (data points with error-bars). For each fixed value of Q_{cut}^2 , we have performed three fits with 2, 4 and 6 parameters. These three points are slightly shifted horizontally so that they are recognizable. The corresponding values of χ^2/dof for each fit are also shown as points without error-bars. By inspecting the plot, we get a feeling about the consistency and quality of these different fits and the differences among the values of $F(0,0)$ can also offer us an estimate of the systematics for the fitting procedure.

Having obtained these 8 plots, we proceed as follows:

- For each of these plots, say the example above, we pick the case with lowest value of χ^2/dof as the final result for $F(0,0)$ together its statistical error in this particular case.
- We further attribute a systematic error arising from the fitting procedure by taking the largest difference in the central values of $F(0,0)$ with comparable χ^2/dof . This then yields the result for $F(0,0)$ with a certain type of dispersion relations on a particular ensemble.
- By comparing the difference in $F(0,0)$ between the two different dispersion relations, we further assign a systematic error, which is taken to be the difference between the two values, arising from the lattice spacing.
- Similar procedure can be applied to χ_{c0} as well.

In such a way, we have obtained the results of $F(0,0)$ and $G(0,0)$ on two ensembles which are explicitly listed below:

$$F(0,0)_{B1} = 0.1283(1)(3)(77), \quad (23)$$

$$F(0,0)_{C1} = 0.1240(4)(13)(68), \quad (24)$$

$$G(0,0)_{B1} = 0.1017(7)(102)(126), \quad (25)$$

$$G(0,0)_{C1} = 0.0907(8)(19)(90), \quad (26)$$

In these expressions, the first error is statistical, the second is the error from the fitting procedure described above and the third one is the finite lattice error estimated from using two different dispersion relations. It is clearly seen that, in all cases, the results are dominated

by systematic errors, especially the finite lattice spacing errors. In fact, two results on two different ensembles are consistent within this estimate of finite lattice spacing errors. We therefore decide not to make any continuum extrapolations. Obviously, computations with more values of lattice spacings will be crucial to nail down these large lattice spacing errors.

To compare with previous lattice computations, we notice that the result for $\Gamma(\eta_c \rightarrow \gamma\gamma)$ is slightly larger than previous result presented in Ref. [9] using the same set of configurations. This difference might come from the fact that the mixing of the η_c and χ_{c0} in the twisted mass setup was not fully disentangled in the previous calculation in Ref. [9]. It is found that, if we were not using properly chosen operator that mix with both the η_c -like and χ_{c0} -like interpolating operators, we would not be able to observe the correct χ_{c0} signal as we have discussed at the end of subsec III A.

Finally, let us convert the results in the form factors into corresponding ones in the decay widths. We simply add all the errors in the form factors in quadrature and neglect the errors in the mass of the mesons. This then leads to the following results for the decay widths:

$$\begin{aligned} \Gamma(\eta_c \rightarrow \gamma\gamma)_{B1} &= 1.62(19) \text{ KeV}, \\ \Gamma(\eta_c \rightarrow \gamma\gamma)_{C1} &= 1.51(17) \text{ KeV}, \\ \Gamma(\chi_{c0} \rightarrow \gamma\gamma)_{B1} &= 1.18(38) \text{ KeV}, \\ \Gamma(\chi_{c0} \rightarrow \gamma\gamma)_{C1} &= 0.93(19) \text{ KeV}, \end{aligned} \quad (27)$$

These are to be compared with the following values given by PDG:

$$\begin{aligned} \Gamma(\eta_c \rightarrow \gamma\gamma)_{PDG} &= 5.02(51) \text{ KeV}, \\ \Gamma(\chi_{c0} \rightarrow \gamma\gamma)_{PDG} &= 2.20(22) \text{ KeV}, \end{aligned} \quad (28)$$

These numbers are all in the same ballpark as the experimental ones though still somewhat smaller. However, since no controlled continuum extrapolations have been performed yet, it is still premature to draw any conclusions for the discrepancy. Our large estimated finite lattice errors offer some hint that this might be the major source of errors. In the future, more studies at different lattice spacing s are needed in order to control the lattice artifacts in a systematic fashion. Another source of systematic error could come from the mixing with the nearby glueball states. So far, no lattice calculations have considered such an effect. Considerable efforts are needed in the future in order to bring these into account.

IV. CONCLUSIONS

In this exploratory study, we calculate the two-photon decay width for η_c and χ_{c0} using unquenched $N_f = 2$ twisted mass fermions. The computation is done with two lattice ensembles (coarser and finer) at two different lattice spacings. The mass spectrum for the η_c and χ_{c0}

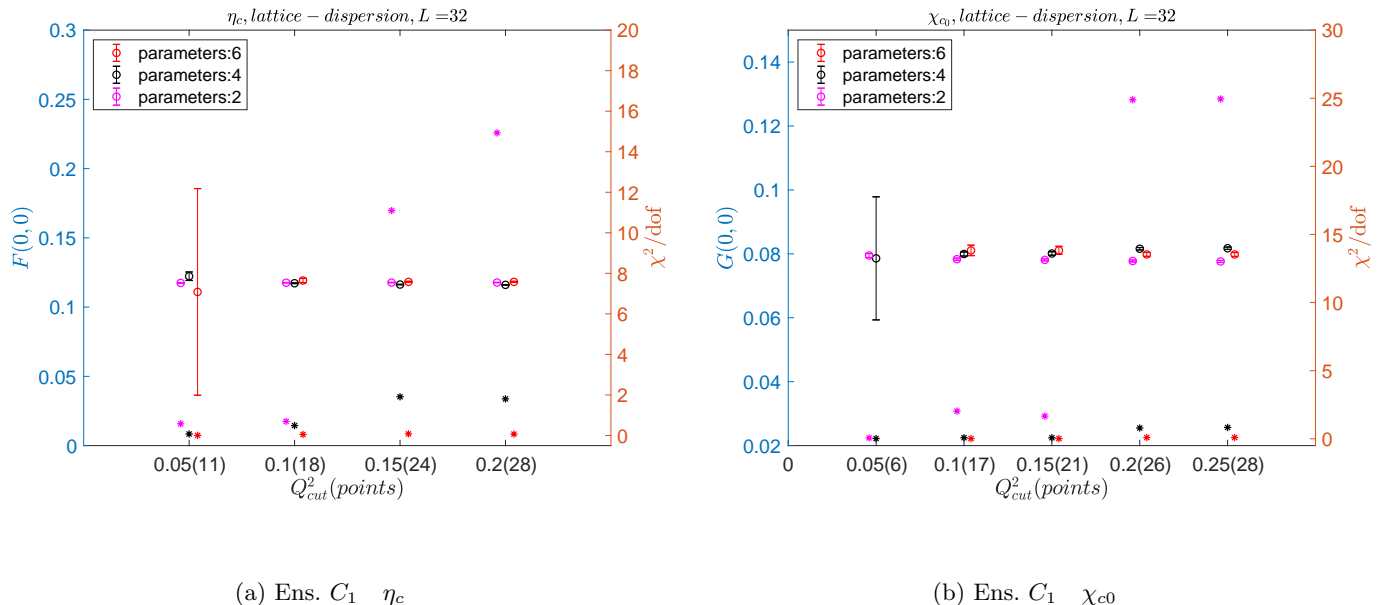


FIG. 8: The fitting results for η_c and χ_{c0} on Ens.C1 using lattice dispersion relations. The horizontal axis denotes the cut values Q_{cut}^2 while the vertical axis indicates the values for $F(0,0)$ or $G(0,0)$ together with the errors (data points with error-bars). The integers in brackets along the horizontal axis indicate the number of data points below Q_{cut}^2 . Points without errors show the corresponding values of χ^2/dof , the values of which is obtained to the right edge of each box.

meson state are obtained by solving a generalized eigenvalue problem which disentangles parity mixing between the two mesons.

Our results for the decay width $\Gamma(\eta_c \rightarrow \gamma\gamma)$ and $\Gamma(\chi_{c0} \rightarrow \gamma\gamma)$ are summarized in Eq. (27) for two ensembles utilized in this computation. With only two ensembles we only estimate the finite lattice spacing errors for each ensemble and no continuum extrapolations are performed. Albeit without the continuum extrapolations, our results are in the right ballpark as the PDG values shown in Eq. (28).

In the future, lattice calculations with more values of lattice spacings are definitely needed so as to control the finite lattice spacing errors which appear to be a dominant source. Meanwhile, the disconnected contributions is a good supplement to this study. Possible mixing with the gluonic excitations should also be studied. It's also helpful to research on unquenched configurations with other ensembles or other methods. We also expect more precise experiments on double-photon decays of charmonium.

Acknowledgments

The authors would like to thank the European Twisted Mass Collaboration (ETMC) to allow us to use their

gauge field configurations. Our thanks also go to National Supercomputing Center in Tianjin (NSCC). This work is supported in part by the National Science Foundation of China (NSFC) under the Project No. 11505132, No. 11335001, No. 11275169, No. 11405178, No. 11575197, No. 11935017, No. 11575196, No. 11875169, No. 11775229. It is also supported in part by the DFG and the NSFC (No. 11261130311) through funds provided to the Sino-German CRC 110 symmetries and the Emergence of Structure in QCD. This work is also funded in part by National Basic Research Program of China (973 Program) under code number 2015CB856700. M. Gong and Z. Liu are partially supported by the Youth Innovation Promotion Association of CAS (2013013, 2011013). This work is also supported by the Scientific Research Program Funded by Shaanxi Provincial Education Department under the grant No. 19JK0391, and Natural Science Basic Research Plan in Shaanxi Province of China (Program No. 2019JM-001).

[1] W. I. Eshraim and C. S. Fischer, Eur. Phys. J. A **54**, 139 (2018), arXiv:1802.05855 [hep-ph]

[2] X. Garcia i Tormo, Mod. Phys. Lett. **A28**, 1330028

- (2013), arXiv:1307.2238 [hep-ph]
- [3] J. M. Cornwall, Mod. Phys. Lett. **A28**, 1330035 (2013), arXiv:1310.7897 [hep-ph]
- [4] J. P. Lees *et al.* (BaBar), Phys. Rev. **D81**, 052010 (2010), arXiv:1002.3000 [hep-ex]
- [5] T. N. Pham, Nucl. Phys. Proc. Suppl. **234**, 291 (2013)
- [6] V. Savinov (Belle), Nucl. Phys. Proc. Suppl. **234**, 287 (2013)
- [7] M. Ablikim *et al.* (BESIII), Phys. Rev. **D85**, 112008 (2012), arXiv:1205.4284 [hep-ex]
- [8] R. Frezzotti, S. Sint, and P. Weisz (ALPHA collaboration), JHEP **0107**, 048 (2001), arXiv:hep-lat/0104014 [hep-lat]
- [9] T. Chen *et al.* (CLQCD), Eur. Phys. J. **C76**, 358 (2016), arXiv:1602.00076 [hep-lat]
- [10] J. J. Dudek and R. G. Edwards, Phys. Rev. Lett. **97**, 172001 (2006), arXiv:hep-ph/0607140 [hep-ph]
- [11] C. J. Shultz, J. J. Dudek, and R. G. Edwards, Phys. Rev. **D91**, 114501 (2015), arXiv:1501.07457 [hep-lat]
- [12] B. Blossier *et al.* (ETM Collaboration), Phys.Rev. **D82**, 114513 (2010), arXiv:1010.3659 [hep-lat]
- [13] Y. Chen, D.-C. Du, B.-Z. Guo, N. Li, C. Liu, *et al.*, Phys.Rev. **D84**, 034503 (2011), arXiv:1104.2655 [hep-lat]
- [14] A. M. Abdel-Rehim, R. Lewis, R. Woloshyn, and J. M. Wu, Phys.Rev. **D74**, 014507 (2006), arXiv:hep-lat/0601036 [hep-lat]
- [15] B. Blossier *et al.* (European Twisted Mass Collaboration), JHEP **0804**, 020 (2008), arXiv:0709.4574 [hep-lat]
- [16] B. Blossier *et al.* (ETM Collaboration), JHEP **0907**, 043 (2009), arXiv:0904.0954 [hep-lat]
- [17] R. Frezzotti and G. Rossi, JHEP **0410**, 070 (2004), arXiv:hep-lat/0407002 [hep-lat]
- [18] M. Kalinowski and M. Wagner, Phys. Rev. **D92**, 094508 (2015), arXiv:1509.02396 [hep-lat]
- [19] M. Tanabashi *et al.* (Particle Data Group), Phys. Rev. D **98**, 030001 (Aug 2018), <https://link.aps.org/doi/10.1103/PhysRevD.98.030001>
- [20] W. Sun, L.-C. Gui, Y. Chen, M. Gong, C. Liu, Y.-B. Liu, Z. Liu, J.-P. Ma, and J.-B. Zhang, Chin. Phys. C **42**, 093103 (2018), arXiv:1702.08174 [hep-lat]
- [21] J. J. Dudek, R. G. Edwards, and D. G. Richards, Phys. Rev. **D73**, 074507 (2006), arXiv:hep-ph/0601137 [hep-ph]